Chapter 4

Electron Transfer Reaction Through an Adsorbed Layer

4.1 Introduction

A proper understanding of electron transfer reaction through an adsorbate intermediate constitutes the first step towards modelling the charge transfer across a chemically modified electrode [172, 173, 174], through a molecular wire [175, 176], or the phenomenon of the molecular electronics [177, 175, 178, 179, 180, 181]. In fact the indirect heterogeneous electron transfer is a recurring feature in all these processes.

In this chapter, the kinetics of an adsorbate mediated electron transfer reaction is considered. The adsorbate is taken to be a metal ion. The reactant is supposed to couple with the adsorbate orbital alone; the direct coupling between the reactant and Bloch states in the metal electrode is neglected. The adsorbate coverage factor θ is allowed to take any arbitrary value in the range $(0, 1)$. Thus starting from a single adsorbate case, corresponding to $\theta \longrightarrow 0$ limit, the formalism remains valid all the way up to a monolayer regime ($\theta = 1$). An important characteristics of metallic adsorbates is that at low coverage, the adsorbate orbital is spatially localized. But in the monolayer regime, one obtains extended electron states in the adlayer. These states form a two-dimensional band [182, 183]. The localized adsorbate state interact strongly with the solvent polarization modes. On the other hand, the interaction of extended electron states with the polarization modes are much weaker, and as a first approximation, it can

be neglected [184] .

A progressive desolvation of adspecies, when the coverage is varied from zero to one, changes adsorbate orbital energy by a few electron volts and hence must leave very significant effects on the electrode kinetics. In addition, in the monolayer regime, the metallic adlayer itself acts as the electrode surface. As a consequence, the adsorbate mediated electron transfer ought to exhibit the characteristics of a direct heterogeneous reaction.

Therefore, a study of how the metallization of an adlayer, and the subsequent desolvation of the adsorbate bridge influences the indirect heterogeneous electron transfer poses a challenging problem in the area of electrode kinetics. In the cited references, the coverage dependent potential energy profile for a bridge mediated electron transfer reactions is generated [184]. In the present chapter, the current-potential relation for such processes is provided and analysed.

The adsorbates exhibit different structural arrangements at different coverage. Even at a fixed coverage, more than one kind of distribution pattern can be observed in the adlayer [185, 186, 187, 188]. Modelling each configuration separately poses a difficult task. Therefore we consider a random distribution of the adsorbates in a two dimensional layer. Subsequently, an 'effective-medium' description is used for the adlayer. This procedure captures the essential features of the adlayer in an average sense [184, 189].

4.2 Model Hamiltonian

An adsorbate has strong electronic coupling with the substrate band states as well as it has electronic overlap with neighbouring adspecies. The latter coupling leads to a two-dimensional band formation in the adlayer at higher coverage. The solvent polarization modes are usually modelled in the harmonic boson approximation and their linear coupling with the adsorbate and reactant lead to solvation and solvent reorganization energies. Here the reactant-adsorbate electronic interation is taken to be weak, thus enabling us to treat it with in the linear response formalism [190]. The model Hamiltonian

representing the physical system is characterized by certain key features to be discussed as follows. Chemisorbed species are distributed randomly on the various adsorption sites on the electrode substrate . Thes sites are considered to form a two-dimensional lattice and are commensurate with underlying substrate. The energy levels associated with the vacant sites are taken to be infinity to ensure that no electron transfer takes place through a vacant site. The random distribution of the adsorbates leads to a randomness in the site energies , that is in a sense, they acquire a random characteristics depending on the occupancy or the vacancy of the site. No randomness is associated with the underlying substrate. Thus the necessary Hamiltonian needed to describe the electron transfer process is shown below [184]

$$\begin{aligned} \mathrm{H} &= \sum_{\sigma} \bar{\epsilon}_r(\{b_\nu + b_\nu^\dagger\}) n_{r\sigma} + \sum_{\sigma} [\upsilon_{ar} c_{a\sigma}^\dagger c_{r\sigma} + h.c] - \sum_{\nu} \lambda_{rc\nu}(b_\nu + b_\nu^\dagger) \\ & \sum_{k,\sigma} \epsilon_k n_{k\sigma} + \sum_{i,\sigma} \hat{\epsilon}_{i\sigma}(\{b_\nu + b_\nu^\dagger\}) n_{i\sigma} + \sum_{\nu} \omega_\nu b_\nu^\dagger b_\nu \\ & + \sum_{k,i,\sigma} [\upsilon_{ik} c_i^\dagger c_k + h.c] + \sum_{i \neq j,\sigma} \upsilon_{ij} c_i^\dagger c_j - \sum_{\{i\},\nu} \lambda_{ic\nu}(b_\nu + b_\nu^\dagger) \end{aligned} \tag{4.1}$$

The redox species labelled r is coupled to adsorbate located at site i=a in the adlayer. The sites in the adlayer are specified by i, while the electrode states are labelled by k. n , $c^\dagger$, c represents the number, creation and annihilation operators for electrons while $b^\dagger$ and b represents the creation and annihilation operators for bosons which model the polarization oscillator modes. ν runs from 1 to 4 labelling the polarization modes corresponding to orientational, vibrational, electronic solvent polarization and surface plasmons respectively and ω_ν represents the associated frequencies. υ is used to denote the coupling strength between the electronic states and λ signifies the strength of adsorbate and redox coupling with the boson modes. The subscripts o and c refers to reactant and adsorbate core.

$$\bar{\epsilon}_r(\{b_\nu + b_\nu^\dagger\}) = \epsilon_r^0 + \sum_{\nu} \lambda_{r\nu}(b_\nu + b_\nu^\dagger) \tag{4.2}$$

$$\hat{\epsilon}_{i\sigma} \equiv \epsilon_{a\sigma}^0 + \sum_{\nu} \lambda_{a\nu}(b_\nu + b_\nu^\dagger) \tag{4.3}$$

ϵ_r^0 and ϵ_a^0 are the energies of redox and adsorbate in gas phase. The expression (4.3) gives the energy of the adsorbate site i when it is occupied. As mentioned before, in case where no adsorbate occupies the site i, the following relation ensures that no charge

transfer takes place through unoccupied sites.

$$\langle \hat{\epsilon}_{i\sigma} \rangle \longrightarrow \infty \tag{4.4}$$

While evaluating the shift in adsorbate orbital energy due to it's coupling to boson, the boson mediated interaction between different sites are neglected. Since only a single species adsorption is considered, a replacement of $\lambda_{i\nu}$ by $\lambda_{a\nu}$ and $\lambda_{ic\nu}$ by $\lambda_{c\nu}$ is followed. Coherent potential approximation is employed to handle the randomness associated with the site energy [189].

4.3 Calculation of current

An examination of the model Hamiltonian shows that, the only possible mechanism for transitions involving redox is provided by the redox-adsorbate coupling terms υ_{ar}. Treating the magnitude of υ_{ar} to be small, the current contribution can be obtained with employing linear response formalism. The microscopic current associated with the electron transfer reaction depends on the average value of the rate of change of electronic occupancy of the redox orbital [190].

$$\mathrm{I} = -e\langle \frac{\partial n_r}{\partial t} \rangle \tag{4.5}$$

$$\mathrm{I} = \frac{e}{\hbar^2} \sum_{\sigma} \int_{-\infty}^{\infty} \langle [V_{I\sigma}^{\dagger}(0), V_{I\sigma}] \rangle dt \tag{4.6}$$

where $V_{I\sigma} = \upsilon_{ar} c_{a\sigma}^{\dagger} c_r$. The first term in the commutator leads to anodic current and the second one gives the cathodic current. The expectation value in the above equation corresponds to a density matrix defined by $\mathrm{H}' = \mathrm{H} - \sum_{\sigma}(V_{Ir}^{\dagger} + V_{Ir})$. Employing Frank-Condon approximation, the anodic current is obtained as

$$\mathrm{I}_A = \frac{e}{\hbar^2} \int_{-\infty}^{\infty} dt \mid V_{ar} \mid^2 \langle \langle c_r^{\dagger}(0) c_r(t) \rangle_F \langle c_{a\sigma}(0) c_{a\sigma}^{\dagger}(t) \rangle_F \rangle_B \tag{4.7}$$

Here $\langle \cdots \rangle_F$ implies an average over electronic degrees of freedom, keeping the bosonic variables as fixed parameters and $\langle \cdots \rangle_B$ denotes the thermal average over boson modes

which are treated in classical approximation. The time correlation function involving $c_{a\sigma}, c_{a\sigma}^{\dagger}$ can be expressed in terms of adsorbate Green's function.

$$\langle c_{a\sigma}(0)c_{a\sigma}^{\dagger}(t)\rangle_F = \frac{1}{\pi}\int_{-\infty}^{\infty}(1-f(\epsilon))e^{i\epsilon\tau/\hbar}(\mathrm{Im}G_{ii})_{i=a}d\epsilon \tag{4.8}$$

$$(G_{ii}(\epsilon))_{i=a} = \langle 0 \mid c_{a\sigma}\langle\frac{1}{\epsilon - \mathrm{H}'}\rangle_{c,i=a}c_{a\sigma}^{\dagger} \mid 0\rangle_F \tag{4.9}$$

$$\langle c_r^{\dagger}(0)c_r(t)\rangle_F = \frac{1}{\pi}\int_{-\infty}^{\infty}e^{-i\epsilon\tau/hbar}\delta(\epsilon-\epsilon_r)d\epsilon \tag{4.10}$$

From the expression (4.9) , it is clear that G_{ii} involves a restricted configuration average denoted by $\langle\cdots\rangle_{c,i=a}$. This implies that while obtaining the configuration average, the site a, which is occupied by an adsorbate and through which the electron transfer takes place, is excluded from the averaging. The occupancy status of the remaining sites are still unspecified. Hence for obtaining the deterministic expression for current, coherent potential approximation is employed. From a physical point of view, this formalism implies that the random adsorbate layer has been replaced by an effective medium and the net effect is one in which a redox is coupled to an adsorbate occupying the site a, and this particular adsorbate is embedded in a two dimensional effective medium.

4.3.1 Estimation of Coherent Potential

As mentioned earlier the randomness inherent in the adsorbate occupancy is handled using coherent potential approximation . Accordingly, the inherent random energy operator $\hat{\epsilon}_{i\sigma}n_{i\sigma}$ in (4.3) is to be replaced by a deterministic operator $k_\sigma n_{i\sigma}$. The coherent potential $k_\sigma(\epsilon)$ is same for all the sites, but depends on the energy variable ϵ. k_σ is determined self-consistently. The required self-consistent equation can be obtained as follows.

$$G_{ij} = G_{ij}^0\delta_{ij} + \sum_l G_{ii}^0 W_{il}G_{lj} \tag{4.11}$$

$$W_{il} = V_{il} + \sum_k \frac{V_{ik}V_{kl}}{\epsilon - \epsilon_k} \tag{4.12}$$

The above equation is obeyed by all GF matrix elements corresponding to sites on two-dimensional lattice. The use of coherent potential for configuration averaging leads to the following result for configuration averaged GF

$$\bar{G} = \frac{1}{\epsilon - W - K(\epsilon)} = \frac{1}{N_{||}} \sum_{u} \frac{1}{\epsilon - k - W(\epsilon, u)} \tag{4.13}$$

The coherent potential operator K has an energy dependency and is deterministic, moreover, it is diagonal in the site basis $\{i\}$, that is $K(\epsilon) = \sum_i k(\epsilon) c_i^{\dagger} c_i$. $N_{||}$ is the number of sites and the summation is over the first brillouin zone. The self-consistent expression for K in the more general context when the energy associated with the vacant site is assumed to be some large ϵ_v but not infinite

$$\frac{\theta}{(\epsilon_a - k)^{-1} - \bar{G}_{ii}} + \frac{(1-\theta)}{(\epsilon_v - k)^{-1} - \bar{G}_{ii}} = 0 \tag{4.14}$$

which in the limit of $\epsilon_v \longrightarrow \infty$ becomes

$$k = \epsilon_a - \frac{1-\theta}{\bar{G}_{ii}} \tag{4.15}$$

Substitution of (4.13) in (4.15) leads to the desired form of self-consistent equation to be used for determining $k_\sigma(\epsilon)$.

$$\bar{G}_{ii} = \frac{1}{N_{||}} \sum_{u} \frac{1}{\epsilon - k_\sigma(\epsilon) - W} = \frac{1-\theta}{\epsilon_{a\sigma} - k_\sigma(\epsilon)} \tag{4.16}$$

The above self-consisten expression for the evaluation of k_σ is exact but requires a tedious summations over the brillouin zone and metal states. These can be further simplified by following the certain assumptions. The assumptions are as follows: (i) The separability of the metal state energy ϵ_k in the direction parallel and perpendicular to the surface. (ii) The substrate density of states in the direction perpendicular to the surface is taken to be Lorentzian, whereas the same is assumed to be rectangular along the surface. (iii) The adsorbate occupies the 'on-top' position on the electrode and is predominantly coupled to the underlying substrate atom. Consequently (4.16) becomes

$$\begin{aligned} \bar{G}_{ii} &= \frac{1-\theta}{\epsilon_{a\sigma} - k_\sigma(\epsilon)} \\ &= \frac{1}{2\Delta_{||}(B-A)\mu} [(A-C) ln \left(\frac{A - \Delta_{||}}{A + \Delta_{||}} \right) - (B-C) ln \left(\frac{B - \Delta_{||}}{B + \Delta_{||}} \right)] \end{aligned} \tag{4.17}$$

$$A/B = \frac{1}{2}[(C+D) \pm \{(C+D)^2 - 4(CD - \frac{\upsilon^2}{\mu})\}^{1/2}] \tag{4.18}$$

$$C = \frac{\epsilon - k_\sigma(\epsilon)}{\mu} \quad ; \quad D = \epsilon - i\Delta_\perp \quad ; \quad \mu = \theta\delta/\Delta_{||} \tag{4.19}$$

δ is the half-bandwidth of the adsorbate monolayer and $2\Delta_{||}$ is the substrate bandwidth at the surface. It should be noted that when the coverage tends to zero the cocnfigurational averaged GF equals θ times the adsorbate GF obtained for the "lone adsorbate" case. Moreover, it can be proven that eventhough μ tends to zero when θ approached zero, the $\bar{G}_{ii}$ remains finite in this limit. This can be verified either by suitable expansion of adsorbate GF, or by a priori taking μ to be zero and reevaluating the adsorbate Green's function. The restricted configurational averaged GF $(G_{ii})_{i=a}$ can be related to the complete configuration averaged GF as

$$(G_{ii})_{i=a} = \frac{1}{(\bar{G}_{ii})^{-1} + k_\sigma - \hat{\epsilon}_{a\sigma}} \tag{4.20}$$

Expressing

$$\bar{G}_{ii}^{-1}(\epsilon,\theta) + K_\sigma(\epsilon,\theta) = X_1(\epsilon,\theta) + iX_2(\epsilon,\theta) \tag{4.21}$$

$$\mathrm{Im}(G_{ii})_{i=a} = \frac{-X_2(\epsilon,\theta)}{[(X_1(\epsilon,\theta) - \hat{\epsilon}_{a\sigma})^2 + (X_2(\epsilon,\theta))^2]} \tag{4.22}$$

In order to evaluate the anodic current I_A, a thermal average over boson modes is to be carried out. Treating them as oscillators in seperate thermal equilibrium, the required density matrix for this average in this limit is

$$\mathrm{P}_{q_\nu} = W(q_\nu) / \int_{-\infty}^{\infty} W(q_\nu) dq_\nu \tag{4.23}$$

$$W(q_\nu) = exp[-\beta \sum_\nu \frac{\omega_\nu}{2}(p_\nu^2 + q_\nu^2) + \bar{\lambda}_\nu q_\nu] \tag{4.24}$$

With the above defined probability function the net expression for anodic current is shown below

$$
\begin{aligned}
I_a &= e\langle n_r\rangle \mid v_{ar} \mid^2 \frac{1}{\sqrt{\pi}\hbar}\frac{1}{\mathrm{Z}}\int d\epsilon \int (\Pi_\nu dq_\nu)\int dt \int d\tau[(1-f(\epsilon)] \\
& exp[-\beta \sum_{\nu=1,2}\frac{\omega_\nu}{2}(p_\nu^2+q_\nu^2)+\bar{\lambda}_\nu q_\nu] \quad exp[i(\epsilon-\epsilon_r-\sum_\nu \lambda_{r\nu}q_\nu)t] \\
& exp[i(X_1(\epsilon,\theta)-\epsilon_a-\sum_\nu \lambda_{a\nu}q_\nu)\tau- \mid X_2(\epsilon,\theta) \mid\mid \tau \mid]
\end{aligned} \tag{4.25}
$$

where

$$
\mathrm{Z} = \int (\Pi_\nu dq_\nu) e^{[-\beta\sum_\nu \frac{\omega_\nu}{2}(p_\nu^2+q_\nu^2)+\bar{\lambda}_\nu q_\nu]} \tag{4.26}
$$

In the above expressions $\bar{\lambda}_\nu = \lambda_{c\nu} + \lambda_{o\nu} + \lambda_{r\nu}$ as the consideration is towards anodic current. A similar expression can be obtained for cathodic current following the same prescription as above. The crucial difference to notice between the anodic and cathodic current is that for cathodic current the $1-f(\epsilon)$ is to be replaced with $f(\epsilon)$ and $\bar{\lambda}_\nu$ for cathodic current is equal to $\lambda_{c\nu}+\lambda_{o\nu}+\lambda_{a\nu}$.

4.3.2 Current expression in terms of re-orangisation energies and overpotentials

Carrying out the various integrations involved in (4.25) the anodic current contribution within the limit of linear response formalism is obtained

$$
I_a \;=\; 2\,e\theta|v_{ar}|^2\sqrt{\pi}\hbar^{-1}\int_{-\infty}^{\infty} sgn(X_2(\epsilon,\theta))\,(1-f(\epsilon))\;\rho_a^{\mathbf{an}}(\epsilon)\,\rho_r^{\mathbf{an}}(\epsilon)d\epsilon \tag{4.27}
$$

Here ϵ_f denotes the electrochemical potential of the system. $\rho_a^{\mathbf{an}}(\epsilon)$ and and $\rho_r^{\mathbf{an}}(\epsilon)$ are the adsorbate and the reactant density of states.

$$
\rho_a^{an}(\epsilon) \;=\; \frac{1}{2\sqrt{\pi P}} Re(w(z)) \tag{4.28}
$$

$$
w(z) \;=\; e^{-z^2} erfc(-iz) \tag{4.29}
$$

$$P = \frac{(4E_a^r E_r^r - (E_{ar}^r)^2)}{4\beta E_r^r} \tag{4.30}$$

$$Z = (-Q^{\mathbf{an}} + i|X_2(\epsilon,\theta)|)/(2\sqrt{P})\,, \tag{4.31}$$

$$Q^{an} = X_1(\epsilon,\theta) - \epsilon_{a\sigma}^0 + \sum_\nu \frac{\lambda_{a\nu}\bar{\lambda}_\nu}{\omega_\nu} - \frac{(\epsilon - \epsilon_r^0 + \sum_\nu \frac{\lambda_{r\nu}\bar{\lambda}_\nu}{\omega_\nu})E_{ar}^r}{2E_r^r} \tag{4.32}$$

in case of anodic current.

$$E_r^r = \sum_\nu \frac{\lambda_{r\nu}^2}{\omega_\nu};\quad E_a^r = \sum_\nu \frac{\lambda_{a\nu}^2}{\omega_\nu};\quad E_{ar}^r = 2\sum_\nu \frac{\lambda_{r\nu}\lambda_{a\nu}}{\omega_\nu}; \tag{4.33}$$

are the reorganization energy for the reactant, adsorbate, and the cross reorganization energy, respectively.

$$\rho_r(\epsilon) = \sqrt{\frac{\beta}{4\pi E_r}}\, exp\left[-\beta\frac{(\epsilon - \epsilon_r')^2}{4E_r}\right] \tag{4.34}$$

Alternatively, we can also write

$$\epsilon_r' = \epsilon_r^0 - \sum_\nu \frac{\lambda_{r\nu}\bar{\lambda}_\nu}{\omega_\nu} = F_R^r - F_O^r - E_r^r \equiv \eta - E_r^r \tag{4.35}$$

where

$$F_R^r = \epsilon_R - \sum_{\nu=1}^4 \frac{\lambda_{R\nu}^2}{\omega_\nu} - 2\sum_{\nu=1}^4 \frac{\lambda_{R\nu}\lambda_{c\nu}}{\omega_\nu} \tag{4.36}$$

$$F_O^r = \epsilon_O - \sum_{\nu=1}^4 \frac{\lambda_{o\nu}^2}{\omega_\nu} - 2\sum_{\nu=1}^4 \frac{\lambda_{o\nu}\lambda_{c\nu}}{\omega_\nu} \tag{4.37}$$

F_O and F_R denote the free energies of the redox-couple in the oxidized and reduced states. $\epsilon_R - \epsilon_O = \epsilon_r^o$, $\lambda_{R\nu} = \lambda_{r\nu} - \lambda_{o\nu}$. Thus $F_R - F_O$ gives the overpotential η for the electron transfer reaction. Similarly, the fraction of overpotential drop between the electrode and adsorbate is related to the change in the adsorbate free energy during the reaction

$$\epsilon_{a\sigma}' = \epsilon_{a\sigma}^0 - \sum_\nu \frac{\lambda_{a\nu}\bar{\lambda}_\nu}{\omega_\nu} = F_R^a - F_O^a - E_a^r \equiv \alpha\eta - E_a^r + E_{ar}^r \tag{4.38}$$

Rewriting the anodic current expression in terms of overpotential, the expression for Q^{an} and ρ_r^{an} takes the form as shown below.

$$Q^{an} \;=\; X_1(\epsilon,\theta) - \alpha\eta - E_a^r + E_{ar}^r - \frac{(\epsilon - \eta + E_r^r)E_{ar}^r}{2E_r^r} \tag{4.39}$$

$$\rho_r^{an}(\epsilon) == \sqrt{\frac{\beta}{4\pi E_r^r}}\, exp\left[-\beta\frac{(\epsilon - \eta + E_r^r)^2}{4E_r^r}\right] \tag{4.40}$$

Proceeding along similar lines of argument for the cathodic current, and noting that $\bar{\lambda}_\nu = \lambda_{c\nu} + \lambda_{o\nu} + \lambda_{a\nu}$ for cathodic current, the expression for Q and ρ_r obtained as shown below,

$$\mathrm{I}_c \;=\; 2\,e\theta|v_{ar}|^2\sqrt{\pi}\hbar^{-1}\int_{-\infty}^{\infty} sgn(X_2(\epsilon,\theta))\, f(\epsilon)\;\rho_a(\epsilon)\,\rho_r(\epsilon)d\epsilon \tag{4.41}$$

$$Q^{cat} \;=\; X_1(\epsilon,\theta) - \alpha\eta + E_a^r - \frac{(\epsilon - \eta - E_r^r + E_{ar}^a)E_{ar}^r}{2E_r^r} \tag{4.42}$$

$$\rho_r^{cat}(\epsilon) == \sqrt{\frac{\beta}{4\pi E_r^r}}\, exp\left[-\beta\frac{(\epsilon - \eta - E_r^r + E_{ar}^r)^2}{4E_r^r}\right] \tag{4.43}$$

The coupling constants between adsorbate and various oscillator modes are scaled by a factor $\sqrt{(1-\theta^2)}$ to take into account the disolvation effect as adlayer itself exhibits metallic properties in the higher coverage regime. Consequently, the solvation and re-organization energy for the adsorbate get scaled by a factor $(1-\theta^2)$, and the solvent induced cross energy terms are scaled as $\sqrt{(1-\theta^2)}$. No such scaling is present for solvation and reorganization energies of the redox-couple. Thus the scaling laws for the various re-organisation are as follows

$$E_{ar}^r(\theta) = \sqrt{(1-\theta^2)}E_{ar}^r(0) \quad ; \quad E_a^r(\theta) = (1-\theta^2)E_a^r(0) \tag{4.44}$$

4.4 Numerical Results and Discussions

The basic concern of this chapter is towards current-overpotential characteristics with

specific emphasis on the variation with the coverage factor (θ) and the fraction of overpotential drop ($\alpha\eta$) across the adsorbate. A first look at the expression for anodic current eq. 4.27 shows that the current is an overlap integral of three terms corresponding to the availability of vacant energy level at the electrode ($1 - f(\epsilon)$), the density of states of the solvated redox couple ρ_r^{an} and the density of states of the adsorbate ρ_a^{an}. The redox density of states has a Gaussian form in terms of ϵ. The self-consistent evaluation of the coherent potential $k_\sigma(\theta)$ enforces a numerical derivation of the adsorbate density of states. However in the following limiting cases, $k_\sigma(\theta)$ takes the value

$$\lim_{\theta \to 0} k_\sigma = \epsilon - \frac{\epsilon - \epsilon_{a\sigma} - w_{ii}}{\theta} - w_{ii} \tag{4.45}$$

and

$$\lim_{\theta \to 1} k_\sigma = \epsilon_{a\sigma} \tag{4.46}$$

where

$$w_{ii} = \sum_k \frac{|v_{ik}|^2}{\epsilon - \epsilon_k} \tag{4.47}$$

.

Consequently, the adsorbate density of states can be analytically obtained in the limits $\theta \to 0$ and 1. Additionally, $\epsilon'_{a\sigma}$ involved in performing the self-consistent evaluation of the coherent potential takes the value as $\alpha\eta - E_a(\theta) + E_{ar}(\theta)$ for anodic current evaluation and $\alpha\eta + E_a(\theta)$ for cathodic current estimation.

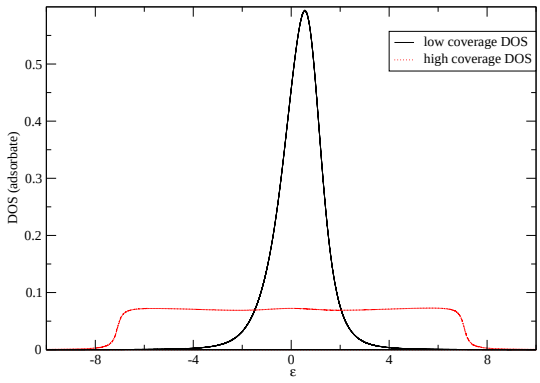

Figure 4.1: Comparison of density of states of the adsorbate for weakly coupled regime at low ($\theta = 0.1$) and high coverage factor ($\theta = 0.9$). The values of parameters (in eV) are as follows: $E_r^r = 0.6, E_{ar}^r(0) = 0.2, E_a^r = 0.4$ and $v = 0.5$ eV.

In what follows, we describe the current vs overpotential profile for different sets of parameters. The adsorbate-electrode interaction is treated both in the weak ($v = 0.5eV$) and strong ($v = 2.0eV$) coupling limits. When the coverage is low, the adsorbate density of states has a single peak Fig. 4.1 . An important consequence of the strong coupling limit is the splitting of the adsorbate level in bonding and anti-bonding states for low θ Fig.4.2. This feature is recaptured in the present analysis since energy dependence of $\Delta(\epsilon)$ is explicitly treated in the present approach On the other hand, the well known wide-band approximation for $\Delta(\epsilon)$ fails to provide the bonding anti-bonding splitting. In the monolayer regime, due to the 2-d bond formation by the adsorbate layer, its density of states acquires a flat profile, irrespective of the strength of the electrode-adsorbate coupling (Fig 4.1, 4.2) . The table I summarizes the values of parameters used in the calculations.

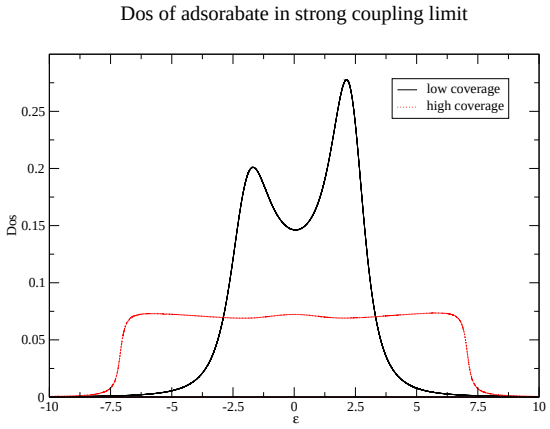

Figure 4.2: Comparison of density of states of adsorbates for strong coupling regime at low and high coverage factor. The values of the various parameters employed (in eV) are as follows: $E_r^r = 1.0, E_{ar}^r(0) = 0.25, E_a^r(0) = 0.75, \Delta_{||} = 1.5, \Delta_{\perp} = 1.5, \mu = 4.5, \upsilon = 2.0$

Table 4.1: Values of parameters used in calculation in eV

	υ	$\Delta_{\|\|}$	$\Delta_{\perp}$	μ	E_r	E_{ar} (0)	E_a (0)
strong	2.0	0.75	1.5	4.5	1.0	0.25	0.75
weak	0.5	0.75	1.5	4.5	0.6	0.2	0.4

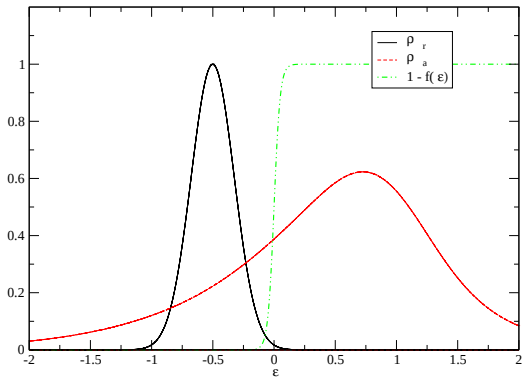

Figure 4.3: Plots showing the density of states for redox, adsorbate and the Fermi distribution for anodic current under zero overpotential. The weakly coupled regime and low coverage of $\theta = 0.3$ is considered here .The values of parameters (in eV) are as follows: $E_r^r = 0.6, E_{ar}^r(0) = 0.2, E_a^r = 0.4$ and $v = 0.5$ eV .

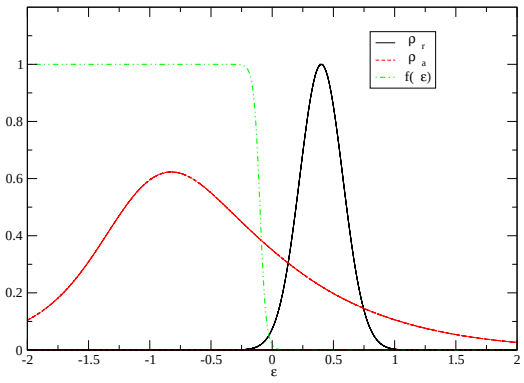

Figure 4.4: Plots showing the density of states for redox, adsorbate and Fermi distribution for cathodic current at zero overpotential. The values of parameters are same as in 4.3

Ideally, under zero overpotential condition, the anodic and cathodic currents are expected to be equal in magnitude. This implies that the profile of the product $\rho_r^{an}(\epsilon)*\rho_a^{an}(\epsilon)$ for anodic current is identical to the product profile $\rho_r^{cat}(\epsilon) * \rho_a^{cat}(\epsilon)$ for the cathodic current. This is a consequence of the equal separation between the peak positions of adsorbate and reactant density of states for anodic and cathodic processes during equilibrium. [Fig. 4.3, 4.4]. The corresponding plots for strongly coupled regime is also shown in Fig. 4.5, 4.6

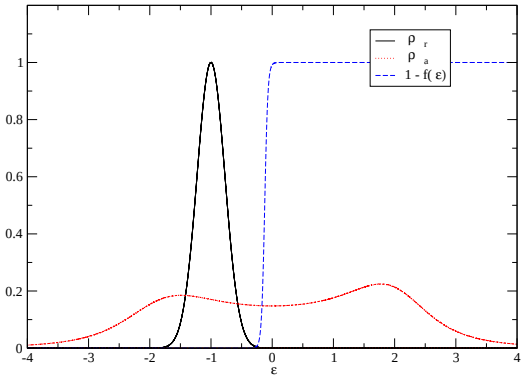

Figure 4.5: Plots showing the density of states for redox, adsorbate and the Fermi distribution for anodic current under zero overpotential. The strongly coupled regime and low coverage of $\theta = 0.3$ is considered here .The values of parameters (in eV) are as follows: $E_r^r = 1.0, E_{ar}^r(0) = 0.25, E_a^r = 0.75$ and $v = 2.0$ eV .

As noted earlier, the electrochemical potential ϵ_f has been set as the zero of energy scale for the direct electron transfer reaction. The presence of additional charge particles for the bridge assisted electron transfer reaction, namely the adsorbates, changes ϕ, the equilibrium potential of the electrode. This is turn gets reflected as a θ dependent variation $\Delta\phi(\theta)$ in $\epsilon_f(\equiv 0)$. The fact that the anodic and cathodic currents at equilibrium potential are identical in magnitude provides a novel method for the determination of $\Delta\phi(\theta)$. Thus the relation $I_a(\eta = 0) = I_c(\eta = 0)$ with $f(\epsilon) = (1 + exp(-\beta(\epsilon + \Delta\phi(\theta)))^{-1}$ (cf eqs. 4.27 and 4.41) enables us to evaluate $\Delta\phi(\theta)$. The variation of $\Delta\phi$ with respect to θ is shown in Fig.4.7 in the limit of weak and strong adsorbate-electrode interaction, with $E_r^r = 0.6$ eV, $E_{ar}^r(0) = 0.2$ eV, $E_a^r\ (0) = 0.4$ eV. The value of $\Delta\phi(\theta)$ depends on the strength of coupling v; its magnitude increases as the coupling becomes stronger.

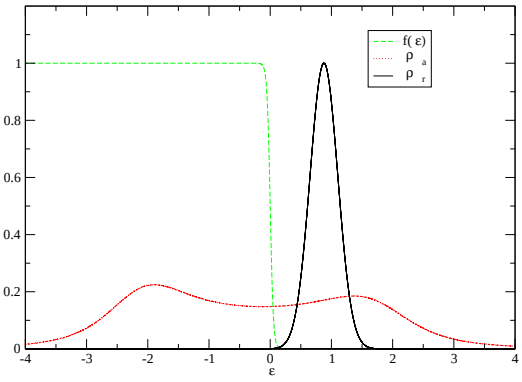

Figure 4.6: Plots showing the density of states for redox, adsorbate and Fermi distribution for cathodic current at zero overpotential. The values of parameters are same as in 4.5

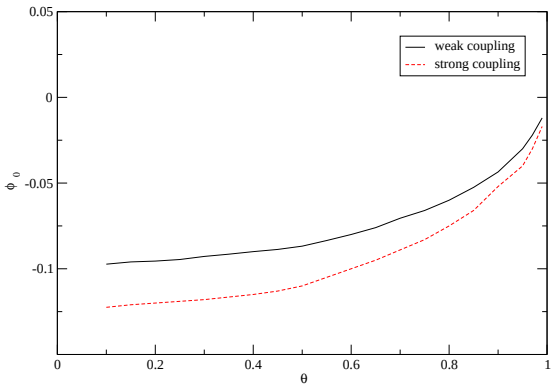

Figure 4.7: Plots showing the variation of $\Delta\phi$ with respect to θ the coverage factor. The values of re-organisation energies employed were same in both the curves. E_r = 0.6 eV, $E_a(0)$ = 0.4 eV, $E_{ar}(0)$ = 0.2 eV

$|\Delta\phi(\theta)|$ is again large for low θ values and remains almost constant in this region. Note that in this regime, the charge on the adsorbate remains localized on the adsorption site. $|\Delta\phi(\theta)|$ starts diminishing sharply for $\theta > 0.6$ and it tends to 0 as $\theta \to 1$. This behaviour is expected. As $\theta \to 1$, the adsorbate layer becomes metallic and gets incorporated in the electrode. The electron transfer acquires the characteristics of a direct heterogeneous reaction, and consequently as noted earlier, the electrochemical potential μ again lies at the zero of the energy scale.

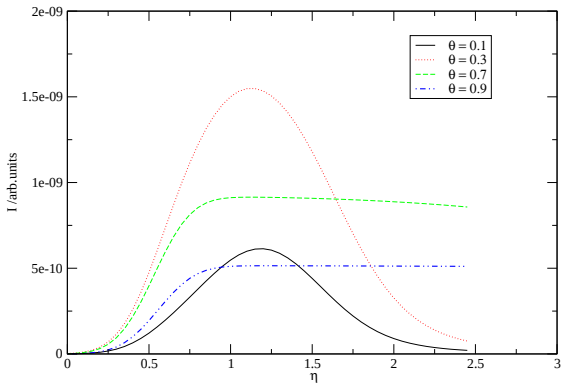

Figure 4.8: anodic current vs η for $\alpha = 0.3$. The values of the various parameters employed (in eV) are as follows: $E_r^r = 1.0, E_{ar}^r(0) = 0.25, E_a^r(0) = 0.75, \Delta_{||} = 1.5, \Delta_\perp = 1.5, \mu = 4.5, \upsilon = 2.0$

We first present the current-overpotential profile in the weak coupling limit ($\upsilon = 0.5\ eV$) for a range of θ and α. The employed values of various reorganization energies are $E_r^r = 0.6$, $E_{ar}^r(0) = 0.2$, $E_a^r\ (0) = 0.4$. The general behaviour can be analysed by looking at the case of lower coverage and high coverage regimes respectively, and then by investigating the effect of variation of α in these limits. Fig. 4.8 shows that for a fixed α, anodic current as well as the current peak height increases with θ in the small θ range ($\theta = 0.1$ and 0.3). This feature arises due to a better overlap between the reactant and adsorbate density of states, whose peak positions are approximately separated by a distance $E_r^r + E_a^r(\theta) - E_{ar}^r(\theta)$. An increase in θ reduces E_a^r and E_{ar}^r (cf eq. 4.44), and hence the peak separation diminishes and the overlap gets enhanced. The presence of anodic current peak at η_p signifies negative differential resistance for $\eta > \eta_p$. This feature

is absent in the higher coverage limit. For large value of θ, the current at higher η exhibits a saturation effect. This is a consequence of the fact that the maximum in the adsorbate density of states ρ_a^{an} is now suppressed. ρ_a^{an} now acquires a plateau profile (Fig 4.1). The plateau height, and therefore the overlap between the reactant and adsorbate density of states decreases with the increasing coverage. Therefore a decrease in the saturation current results as $\theta \to 1$ (curve $\theta = 0.7$ and 0.9 in Fig. 4.8).

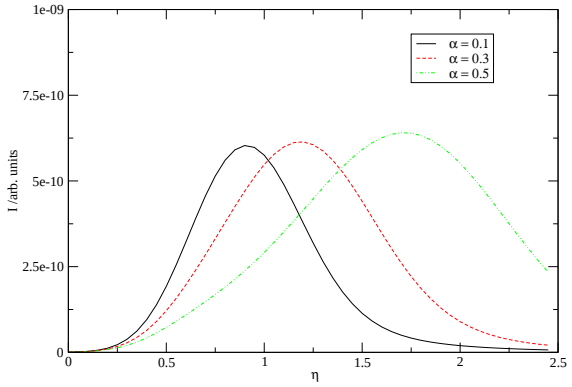

Figure 4.9: anodic current vs η for $\theta = 0.1$ in the weak coupled regime. The values of parameters (in eV) are as follows: $E_r^r = 0.6, E_{ar}^r(0) = 0.2, E_a^r = 0.4$ and $v = 0.5$ eV.

The effect of the α variation on the anodic current is highlighted in Fig. 4.9, 4.10 and 4.11. This effect is more pronounced in the low coverage regime due to the presence of adsorbate density of states peak. The reactant and adsorbate density of states peak separation increases with the increasing α. Consequently, the maximum overlap between the two occurs at larger η. This explains the occurrence of the anodic current peak at higher η values as α increases . On the other hand, the near constant adsorbate density of states for large θ ensures a minimal effect of α variation on the anodic current (Fig. 4.11, 4.12).

Next the strong coupling limit with [$v = 2.0$ eV, $E_r^r = 1.0$ ev, $E_{ar}^r(0) = 0.25$ eV, E_a^r (0) $= 0.75$ ev]is considered. Figures 4.13, 4.14, 4.15 and 4.16 shows the current overpotential response in the strong coupling regime. As in the case of low coverage, the I_a *vrs* η plot exhibits a negative-differential region (Fig. 4.13, 4.14).

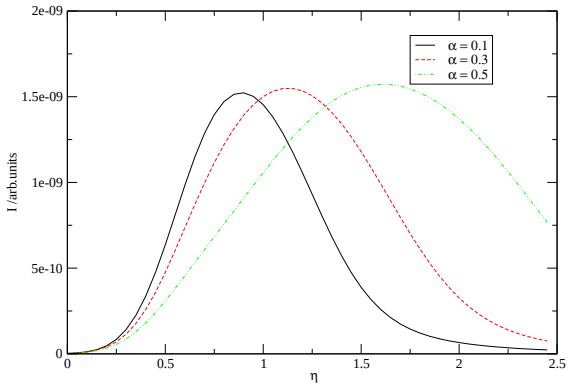

Figure 4.10: anodic current vs η for $\theta = 0.3$ in weak coupled regime. The values of parameters (in eV) are as follows: $E_r^r = 0.6, E_{ar}^r(0) = 0.2, E_a^r = 0.4$ and $v = 0.5$ eV.

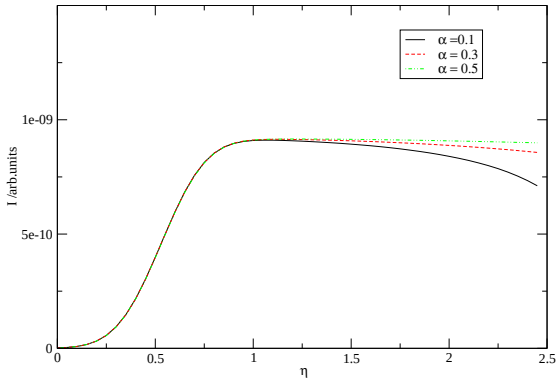

Figure 4.11: anodic current vs η for $\theta = 0.7$. The values of parameters (in eV) are as follows: $E_r^r = 0.6, E_{ar}^r(0) = 0.2, E_a^r = 0.4$ and $v = 0.5$ eV.

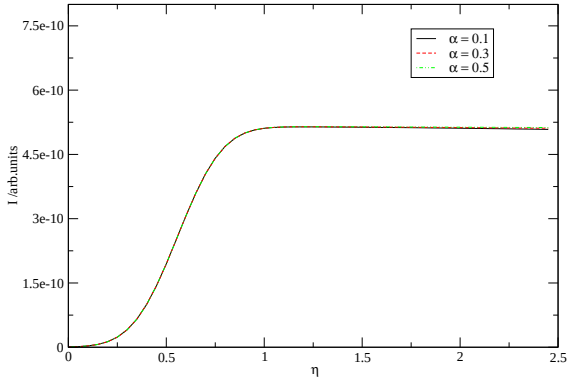

Figure 4.12: anodic current vs η for $\theta = 0.9$. The values of parameters (in eV) are as follows: $E_r^r = 0.6, E_{ar}^r(0) = 0.2, E_a^r = 0.4$ and $v = 0.5$ eV.

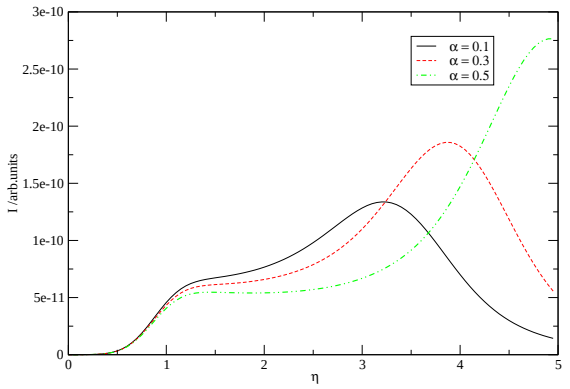

Figure 4.13: anodic current vs η for $\theta = 0.1$. The values of the various parameters employed (in eV) are as follows: $E_r^r = 1.0, E_{ar}^r(0) = 0.25, E_a^r(0) = 0.75, \Delta_{||} = 1.5, \Delta_{\perp} = 1.5, \mu = 4.5, v = 2.0$

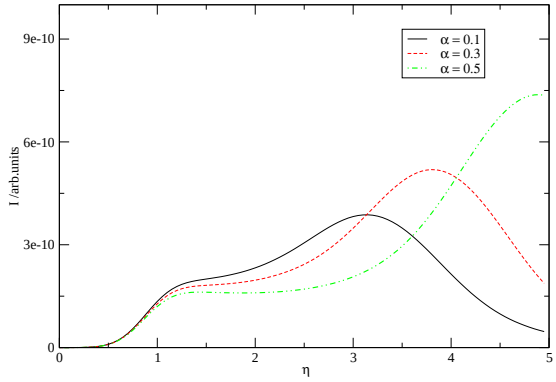

Figure 4.14: anodic current vs η for $\theta = 0.3$.The values of the various parameters employed (in eV) are as follows: $E_r^r = 1.0, E_{ar}^r(0) = 0.25, E_a^r(0) = 0.75, \Delta_{||} = 1.5, \Delta_{\perp} = 1.5, \mu = 4.5, \upsilon = 2.0$

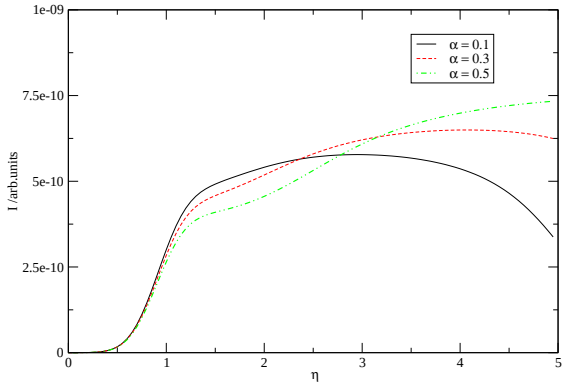

Figure 4.15: anodic current vs η for $\theta = 0.7$. The values of the various parameters employed (in eV) are as follows: $E_r^r = 1.0, E_{ar}^r(0) = 0.25, E_a^r(0) = 0.75, \Delta_{||} = 1.5, \Delta_{\perp} = 1.5, \mu = 4.5, \upsilon = 2.0$

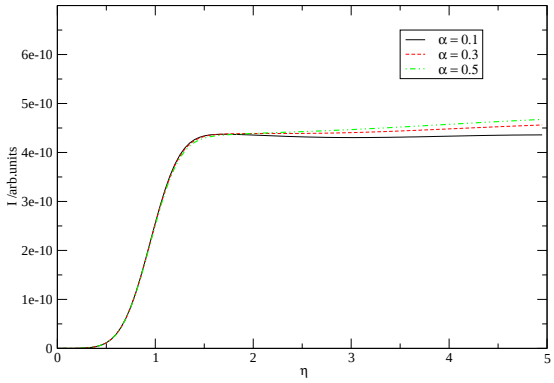

Figure 4.16: anodic current vs η for $\theta = 0.9$. The values of the various parameters employed (in eV) are as follows: $E_r^r = 1.0, E_{ar}^r(0) = 0.25, E_a^r(0) = 0.75, \Delta_{||} = 1.5, \Delta_\perp = 1.5, \mu = 4.5, \upsilon = 2.0$

More importantly, the presence of two peaks in ρ_a^{an} when coupling υ is large and θ is small (Fig. 4.2) leads to a saddle point and a maximum in the I_a vrs. η plot. For the set of parameters currently employed, the $I_{a,Max}$ now occurs at a much larger η in comparison to the weak coupling limit, and may not be accessible experimentally. However, the saddle point in the current appears in an overpotential range where the anodic current peak appears in the weak coupling limit. For large coverage, current potential profile are similar in strong and weak coupling limit. Interestingly, the saturation current is smaller in the large coupling case due to a decrease in the height of ρ_a^{an}. In fact this lowering of the current in the strong coupling holds true for any coverage and η. This is shown in Fig. 4.17 wherein the variation of equilibrium current I^o with respect to coverage is plotted. The I^o is smaller for larger υ, and as explained earlier in the context of Fig. 4.8, shows a maximum in the intermediate coverage regime. However it may be noted that when $\upsilon \to 0$, current would be proportional to $|\upsilon|^2$, and an increase in υ in this very weak coupling limit will lead to an increase in the current.

The high coverage regime of $\theta \to 1$ corresponding to a formation of monolayer of a decrease in the current for higher η when the coverage is low virtually mimics the Marcus inverted region for a homogeneous electron transfer reaction. On the other hand, the current getting saturated at higher η when the coverage is large is also true for a direct

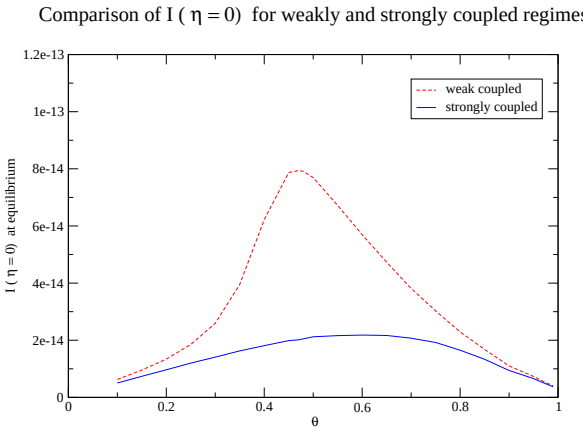

Figure 4.17: Plots showing the equilibrium current at zero overpotential I_0 vs θ for strong and weak coupled regime. The values of re-organisation energies were selected be the same for both the curves, $E_r = 0.6$ eV, $E_a(0) = 0.4$ eV, $E_{ar}(0) = 0.2$ eV

heterogeneous electron transfer reaction. Thus depending on the extent of coverage, an adsorbate mediated electron transfer at an electrode exhibits the characteristics of both homogeneous and heterogeneous electron transfer reactions. The localization of adsorbate electron at low coverage and its delocalization at high coverage is the reason behind this phenomena.

4.5 Summary and Conclusions

In this chapter, we considered electron transfer in an electrochemical system, from a solvated redox to an electrode mediate by intervening adsorbate atoms. Further randomness is introduced in the model in terms of the coverage factor which relates to the number of adsorbate atoms adsorbed on the electrode surface. The theory developed is valid for a range of regime, lone adsorbate mediate transfer to the monolayer formatted direct electron transfer regime. The inherent randomness involved in the adsorbate distribution on the surface has been tackled by coherent potential approximation (CPA) and separate expression are derived for anodic and cathodic current.

Explicit attention was paid to the low coverage and high coverage regime, even though the formalism is valid for all regime, since at these two regions the theory could be compared with pre-existing literature. Plots were also provided for intermediate regimes and additionally, the effect of the adsorbed atoms on the Fermi level of the electrode were incorporated by means of a shifted equilibrium potential $\Delta\phi(\theta)$, ensuring that the anodic and cathodic current were equal under zero overpotential condition.

The analysis also provides a novel method for determining the variation in $\Delta\phi(\theta)$ with changing adsorbate coverage.

The fraction of overpotential drop across the electrode-adsorbate is incorporated and the collective plots are analysed. We have proved that this fraction of overpotential drop plays a significant role in determining the response behaviour of current, typically the location and extent of the maximas in case of lower coverage situations. while in case of high coverage regime, the effect is not profound and the electron transfer follows the traditional direct electron transfer as expected from heuristic arguments.

The dependence of anodic current in the weak and strong electrode-adsorbate coupling is analyzed. In the former case, I_a vrs overpotential profile exhibits a peak, where as in the later case, and in the same overpotential region, the current plot shows a saddle point behaviour. This fact can be used to distinguish a weakly chemisorbed bridge from a strongly chemisorbed one. These distinguishing features occur only when the coverage is low. At high coverage, $I_a \sim \eta$ plots have identical profile for weak and strong coupling cases

At low coverage, it is possible to recover the Marcus inverted region, which is absent when the coverage is large. The localized nature of the adsorbate orbital when coverage is low, and its getting delocalised for high coverages leads to this behaviour.